U.S. Department of Energy Collegiate Wind Competition: Technical Design Report 2020

Written by:

Trevor Brown
Samantha Kruschke
Adrian Nguyen
Mariah Smith
Samuel Rodriguez
John Wang
Forrest Eagle
Casey Jo
Jeffrey Skarin
Taylor Sprague
Andres Vargas

Project Advisors: Dr. Tom Nordenholz, Dr. Evan Chang-Siu, Steffan Long
CSU - Maritime Academy
May 15th, 2020

Table of Contents

Chapter 1: Executive Summary

The objective of this year's team was to improve performance at low windspeeds. As a team, we decided the best way to accomplish this was with a complete redesign of the turbine system used in the previous two competitions. The turbine this year features a 3-blade variable pitch design, a custom generator, a resistive load, and a passive yaw system.

The airfoils selected for this year's blades were the ISA 961 as the primary airfoil and the Rutan AMSOIL Racer wing as the secondary airfoil. The ISA 961 showed great promise in its ability to maintain a consistent power output across a wide range of turbine RPM and its high coefficient of power. As a pair, these airfoils share a similar angle of attack which should allow for smooth operation of the blades.

The variable pitch design will be the primary method for controlling the turbine's power output and rotor speed. The ability to feather the blades out of the wind will also allow for the turbine to brake. The variable pitch mechanism will be operated by a linear actuator mounted to the nacelle. A variable pitch design was chosen because it allows for a passive control system before the turbine reaches its rated power which reduces complexity and power consumption.

One of the major design decisions to improve cut-in performance was to implement a custom generator created by the engineering team. This is the first year that Cal Maritime built a custom generator. The generator to be used has a 3-phase AC radial flux design. It is made completely out of PLA which eliminates cogging torque and greatly reduces the windspeed required to cut in. Most notable, the generator features a Halbach array arrangement for the permanent magnets in the rotor, which allows it to generate the highest power compared to every other design tested.

Another attempt to improve cut-in performance is to use a resistor as an electrical load which is also a first for Cal Maritime. In the past, Cal Maritime has always needed a battery to power the active control system during startup. This would cause negative power to be measured by the PCC during startup. A resistive load will eliminate the negative power draw and allows for all of the power generated at low windspeeds to be measured by the PCC and dissipated by the load.

A drawback to our turbine design is that there is no simple solution to return the turbine blades to the run position after a successful brake. We plan to overcome this challenge by implementing a second control system in the load. The load control system will be able to detect a successful brake and switch the load to a battery that will temporarily power the electrical system and linear actuator until the system can power itself.

Chapter 2: Blade Design

2.1 Initial Screening

Two airfoils were selected to construct our turbine blades: the ISA 961 and the Rutan AMSOIL Racer airfoil. These airfoils were selected based on their promising characteristics and their potential ability to work well together as a seamless pair, mimicking the design choices from the 2019 Maritime team[1]. Using the 2018 Cal Maritime airfoil selection as a baseline, airfoils of the same family as the GOE 195 were screened and the ISA 961 was selected on its slightly higher C_l/C_d value, 40.08, than the 195[2]. The Rutan was found via screening for specific thickness and camber criteria in Airfoil Tools. The ISA 961 has a thickness to chord ratio of 9.3% and a maximum camber of 4.6%. The Rutan airfoil has a thickness to chord ratio of 11.8% and a maximum camber of 1%[3]. This airfoil is strictly for providing structural integrity and complements the angle of attack of the ISA 961 ensuring smooth performance.

2.2 Design

The analysis for the airfoils was done using QBlade, an open source software available for download online. This program uses BEM theory and XFOIL to analyze the airfoils and rotor and produces graphs of their theoretical performance. To start, a Reynolds number must be input into the program before any analysis is run The Reynolds number changes along the length of the blade as the chord changes so an average Reynold number is used. Noting the lower air density in Denver, CO, the estimated Reynolds number was determined to be about 48,000. Using this information, QBlade can then produce a variety of plots for individual airfoils, with those most critical being the coefficient of lift (C_l) versus the angle of attack (α), coefficient of lift over coefficient of drag (C_l/C_d) versus angle of attack, and the coefficient of moment (C_m) versus angle of attack. For a full turbine blade to be made, an optimal α needs to be identified at the largest C_l/C_d. Using this α and a desired design tip speed ratio (TSR), Schmitz optimization can be used to generate blade geometry. The TSR, a unitless value, is the rotational speed of the tip of the blade divided by the wind speed.

Schmitz optimization uses a series of equations to determine the ideal chord and twist of the blade along each section of the blade in order to maximize the power captured from the wind. Using an Excel spreadsheet, a table like table 2.1 can be made and entered into QBlade. The equations used in the Schmitz optimization can be seen below.

$$\varphi = \frac{2}{3}\tan^{-1}\left(\frac{1}{\lambda_r}\right) \qquad c = \frac{8\pi r}{BC_l}(1-\cos\varphi) \qquad \theta_p = \varphi - \alpha$$

Equation 2.1 *Equation 2.2* *Equation 2.3*

In Equation 2.1, φ is the angle of the relative wind to the chord line of the airfoil and λ_r is the local TSR. For Equation 2.2, c is the chord, r is the radial distance from the center of the turbine, B is the number of blades, and C_l is the coefficient of lift. Lastly, for Equation 2.3, θ_p is the measure of twist in the blade at the local radial distance along the blade, and α is the initial design angle of attack[4].

Section	Radius (m)	Chord (m)	Twist θ_P (°)	TSR λ	Airfoil
1	0.0254	0.0492	35.3718	0.5644	Rutan
2	0.0454	0.0489	24.8478	1.0080	Blend
3	0.0653	0.0424	18.0424	1.4516	Blend
4	0.0853	0.0360	13.5463	1.8951	Blend
5	0.1052	0.0309	10.4342	2.3387	ISA 961
6	0.1252	0.0268	8.1798	2.7822	ISA 961
7	0.1452	0.0236	6.4824	3.2258	ISA 961
8	0.1651	0.0211	5.1630	3.6693	ISA 961
9	0.1851	0.0190	4.1104	4.1129	ISA 961
10	0.2050	0.0173	3.2523	4.5564	ISA 961
11	0.2250	0.0158	2.5400	5.0000	ISA 961

Table 2.1 Final Blade Geometry

2.3 Blade Analysis

After the geometry was optimized, one plot from QBlade was then found: coefficient of power (Cp) versus TSR. C_p is a nondimensionalized measure of the mechanical power being extracted from the wind by the turbine blade. This became the prime point of comparison between the GOE 195 airfoil from the 2018 Maritime team and the SD 7080 airfoil from the 2019 team[1][2]. The ISA 961 had a slightly larger Cp than both foils, 0.5018, hence its selection as the primary airfoil for the 2020 design. Perhaps most critically, a key feature that was noted with the ISA 961 was how flat the peak of its Cp versus TSR curve was. This indicates a high degree of controllability in which the turbine can spin at a range of rotational speeds whilst

maintaining a largely constant power output. It was a qualitative comparison in seeing how the GOE 195 and the ISA 961 compared in that respect and the 961 looked to show a smoother peak than the 195. The Rutan airfoil was selected largely for its slightly larger thickness than the ISA 961, thus allowing it to maintain better structural integrity at the root of the blade. With the limited time that ended up being available this year, the iterative testing process that would normally happen was cut short, and table 2.1 shows the turbine blade that was initially manufactured and tested in our wind tunnel. It has since become the "final" blade due to the lack of testing of additional models that had been originally scheduled.

2.4 Variable Pitch

The focus this year was to develop an effective variable pitch system as the primary control mechanism of the turbine. In team design discussions, the conclusion that had been reached was that previous turbine designs by Maritime had reached its zenith and new directions should be explored. As part of this, we conducted an analysis to see how the Cp of a turbine would change as the pitch changes. Looking to Figure 2.2 below, the range of pitch angles goes from -20 degrees to 0 degrees in steps of 4 degrees. This highlights the ability of a variable pitch system to feather the blades out of their optimal position to extract less power out of the wind. With the blades feathered out to higher pitch angles, the turbine will be able to come to a safe halt.

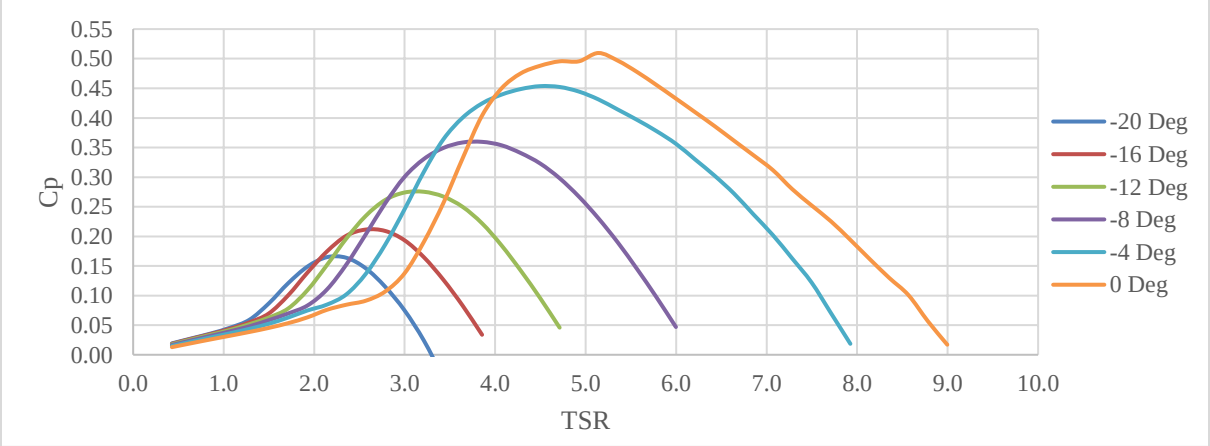

Figure 2.2 Cp vs TSR curves for a range of pitch angles

2.5 Manufacturing

To construct the blades, the geometry from the Schimtz optimization is entered into QBlade to generate an initial model. These QBlade models do not have a root, which must be added in another program. The QBlade model is then exported as an STL file and opened in SolidWorks. In SolidWorks we can add a root feature to the blade that acts as the attachment point to the hub of the turbine. The model can then be saved and transferred to the MakerBot Print software for preparation for printing. The turbine blades we used were manufactured using a MakerBot Replicator+ 3D printer. The material used for the printing process was polylactic acid (PLA) filament, at an infill of 95%, the maximum infill allowed on the current MakerBot Print software.

2.6 Stress Analysis

Perhaps one of the more critical steps in the design of our turbine blades is the stress analysis. We sought to predict the stress and deflection the turbine blades would undergo in an extreme wind situation. Two different analyses were considered to predict the stress and deflection including the combined stress through the length of the blade from centrifugal and aerodynamic loading and the pull-out force at the root due to centrifugal forces. As an initial projection, we calculated the stress through a blade based on a wind velocity of 18 m/s and a rotational speed of 5000 RPM. For this analysis we treated the blades as fixed beams. Using approximation equations, we could determine the area and moment of inertia at each section of the blade along its entire length[5]. Following that, we performed a series of integrations along the length of the blade to determine the shear force, moments, and finally stresses through the length of the blade. Using data from QBlade, we found shear by taking the integral of the normal force through the blade with respect to radial position. The axial force was found by multiplying the axial acceleration and mass of the blade at their respective positions along the length of the blade. We could then take the integral of the shear forces with respect to radial position to find the moment acting at each position along the blade. The initial calculations made showed that the blades would experience a maximum stress of 12.5 MPa from flap-wise loading and centrifugal forces. Experimental data gathered from tensile tests on PLA wishbone samples in our materials lab measured a minimum tensile strength of 38 MPA. This gives the blade a factor of safety of 3.05 for the centrifugal and aerodynamic loading through the length of the blade.

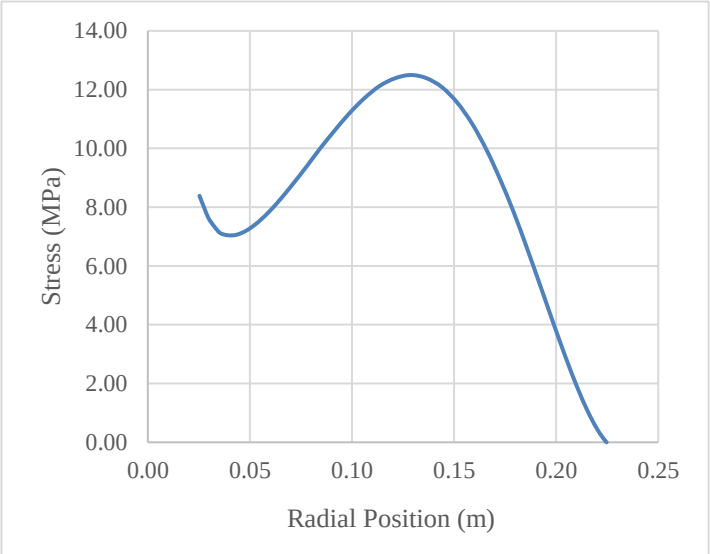

Figure 2.4 Blade Stress vs Radial Position

Another analysis that was performed was seeing how much the blade would deflect along its length. Once again treating the blade as a fixed beam, we used Euler-Bernoulli beam theory. This theory assumes a stationary beam, which the blades are not. As such, the theory fails to take into account the centrifugal forces being applied through the length of the blade that end up helping straighten the blade out and resist deflection. For a wind velocity of 18 m/s, we would see a downwind tip deflection of about 4.25cm.

The pullout force on the root attachment at 5000 RPM was found to be 484 N using the centripetal force analysis discussed previously. We could then use this force in calculating the tensile and shear stresses in the root. The planes of these stresses are shown in Figure 2.5. The dimensions of the shear planes in the root are defined by the variables *x*, *y*, and *z* in Equations 2.4, 2.5, and 2.6. In Equation 2.4, t is the thickness of the airfoil. Looking to Equation 2.5, τ is shear stress and F_n is the normal force. In Equation 2.6, σ is the axial stress and K_t a stress concentration factor, 3.29[6]. The shear stress in this calculation was determined to be 2.21 MPa

and the axial stress 12.48 MPa. Noting the ultimate tensile stress of the PLA was 38 MPa, this gave us a safety factor of 8.60 and 3.04 for shear and axial stress, respectively.

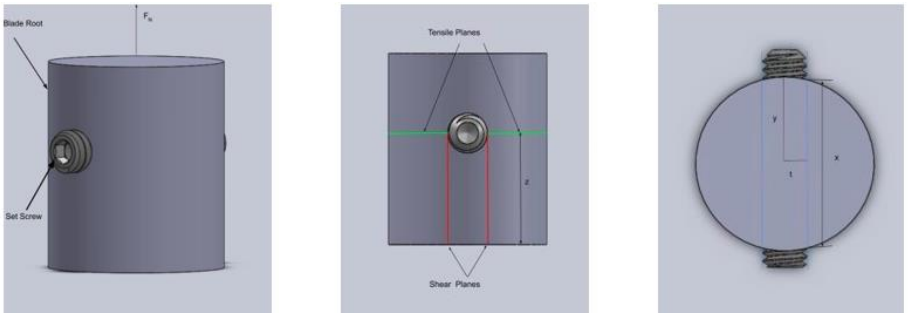

Figure 2.5 Isometric, side, and top view of the male root assembly

$$x = 2\sqrt{y^2 - t^2}$$
Equation 2.4

$$\tau = \frac{F_N}{2xz}$$
Equation 2.5

$$\sigma = \frac{4K_t F_N}{\pi y^2}$$
Equation 2.6

The strength of the turbine blades under a similar loading condition was able to be tested practically. As part of the rotor strength milestone, we set up a test with a similar set of turbine blades to run a turbine with no load in our wind tunnel. Wind speeds reached 13.5 m/s and turbine rotational speeds reached as high as 4700 RPM. Our wind tunnel is unable to reach higher wind velocities, but the rotational speed was close to the speed used in our calculations. Upon completion of the test, the blades were given a visual inspection and there were no obvious signs of cracks in them. It should be noted that PLA has little to no plastic deformation before ultimate failure.

Chapter 3: Mechanical Design

3.1 Overview

An exploded view of the turbine can be seen on the cover of this report. We chose to design a three-blade, variable-pitch turbine with a passive yaw system. All metallic components of the base, tower, generator foundation, tail root, and variable-pitch assembly are to be made of 6061 aluminum. The variable-pitch components were manufactured on a Hass CNC mill. The nacelle was manufactured on a manual mill and the adaptor for the variable-pitch shaft to generator was manufactured on a manual lathe.

3.2 Variable-Pitch

There are five main pieces that make up the variable pitch assembly: the base hub, three blade mounts, three pitch levers, the pitch driver, and the actuator connection clip**.** The base hub design is very similar to the hub of a fixed pitch design, but there is no way to mount the blade on the base hub. Instead there is a place for a bushing and the blade mount piece. The blade mount is the piece where the blade mounts. The pitch levers connect the blade mounts to the pitch driver. The pitch driver is the piece that will be moving axially along the base hub, pushing all three pitch levers and in turn rotating all three blade mounts simultaneously. The actuator connection clip is the only piece in this assembly that is not spinning with the turbine. This piece is connection to the pitch driver with a 5/8” shaft ball bearing. The inside of the ball bearing spins with the pitch driver while the outside stays stationary and connects to the actuator connection clip.

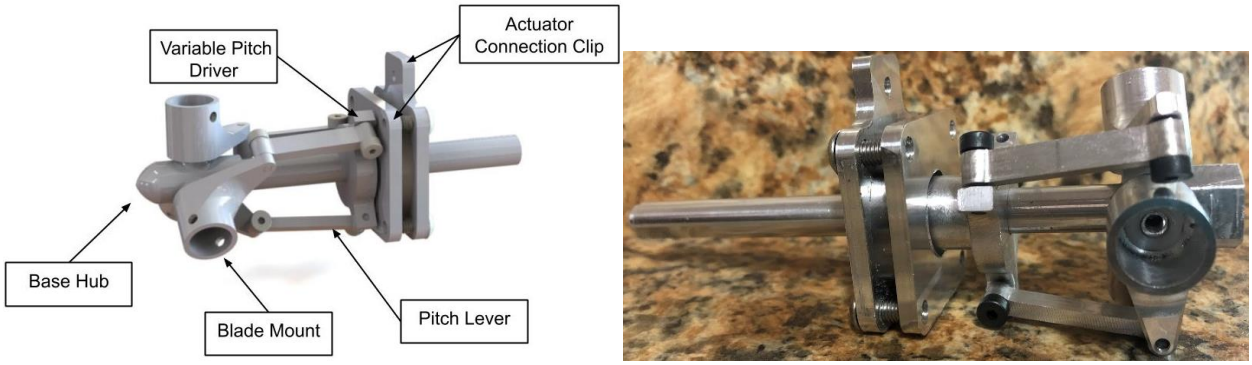

Figure 3.1 Variable pitch assembly SolidWorks (left) & actual (right)

The blade mount will be secured to the base hub and the pieces will be separated by a nylon bushing to prevent the rubbing of metal on metal. It was decided that a bearing was not needed for this because of the limited amount of rotation the blade mount will encounter. The blade mount will be secured to the pitch lever using a 1/8 inch precision shoulder screw, which threads into the blade mount. The pitch lever will also be secured to the pitch driver using a 1/8 inch precision shoulder screw, which threads into the pitch driver. Shoulder screws allow the pieces to be secured together but also rotate freely. The base hub will be secured to the generator shaft using a 3/8 inch female to 8 mm adaptor.

3.3 Nacelle

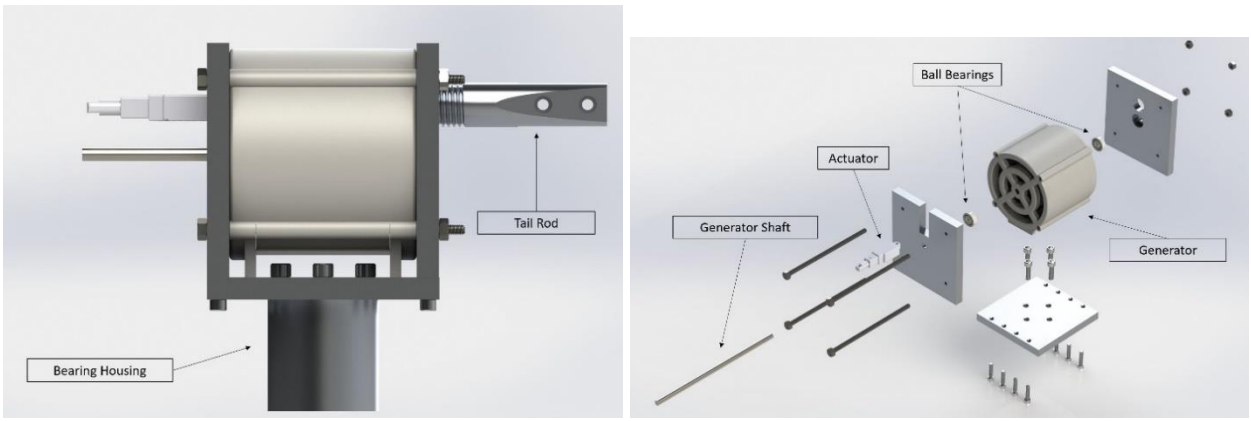

Figure 3.6 Side view of Nacelle (Left) & Exploded view of Nacelle (Right)

The purpose of the nacelle is to support the weight of the generator, secure the actuator, and act as a link by connecting the tail and tower. Figure 3.6 shows the side view and exploded view of the nacelle. The nacelle is made up of three aluminum 6061 plates. The generator is mounted onto both vertical plates via four ¼-20 steel all-thread rods and eight ¼-20 steel hex nuts. Within the inner side of each vertical plate, a counter bore was made in order to house two 8 x 22 x 8-mm ball bearings. This ball bearing placement allows for the weight of the turbine's variable pitch assembly and the generator's rotor to be transferred onto the plates rather than the generator's PLA rotor. An aluminum 6061 8-mm shaft rotates the generator's rotor. A squared slot of the front plate was cut out so that the actuator could properly be held in place. The actuator itself is attached to the front plate with nuts and screws that came as attachments. The tail rod is connected to the back plate via a 1.0-8 threaded hole, located above the shaft. The vertical plates are joined by a horizontal bottom plate via eight ¼-20 socket head screws. The

generator hovers above the bottom plate since attaching it would likely cause over constraining issues. The bottom plate and bearing housing are jointed together via four 5/16-18 screws.

3.4 Passive Yaw & Tower Assembly

A passive yaw system will be utilized to ensure our turbine's blades are always positioned toward the wind. The system consists of a yaw assembly and the tail assembly. This design is heavily influenced by last year's design. The passive yaw system begins with the tail assembly as shown in Figure 3.7 and is broken down into three pieces, the tail fin, tail connecting rod, and two head socket screws/hex nuts. The tail fin and connecting rod are fastened via the two head socket screws/hex nuts. The connecting rod is threaded and screws directly into the back plate of the nacelle. The second part of yaw systems is the tower assembly, shown in Figure 3.8. The aluminum bearing housing is connected beneath the nacelle's bottom plate via four 5/16-18 screws. A 3/4" shaft-diameter ball bearing is wedged between the bearing housing and the tower connection, which allows the turbine to correctly orient the rotor relative to the wind direction. The tower shaft screws into the tower connection, holding it in place.

The passive yaw system continuously works to keep the direction of the rotor parallel to the direction of the wind. If the oncoming wind's direction is changed, the tail will shift off streamline. This will create an aerodynamic moment that corrects the shifted tail back into alignment.

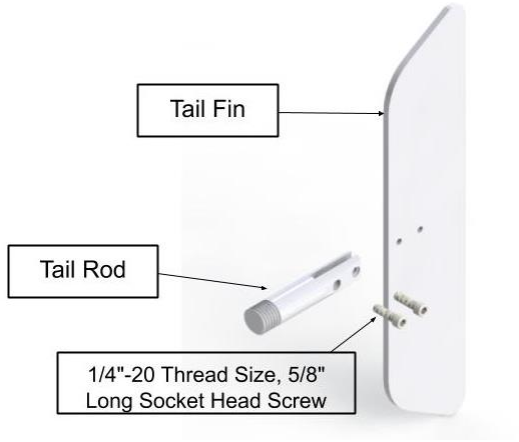

Figure 3.7 Tail assembly

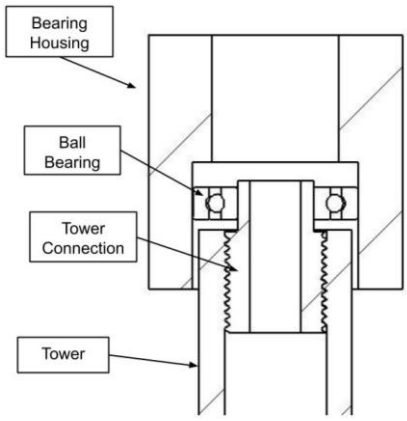

Figure 3.8 Tower assembly sectional view

3.5 Actuator

Since we wanted to use variable pitch for our design this year, it was necessary to determine the correct actuator size. There are many factors that contribute to the amount of force necessary to move the blades including the windspeed, rotational speed, blade geometry, blade angle, density of the air, and the geometry of the pitch mechanism. Using a free body diagram of the pitch mechanism as shown in Figure 3.9, Equation 3.1

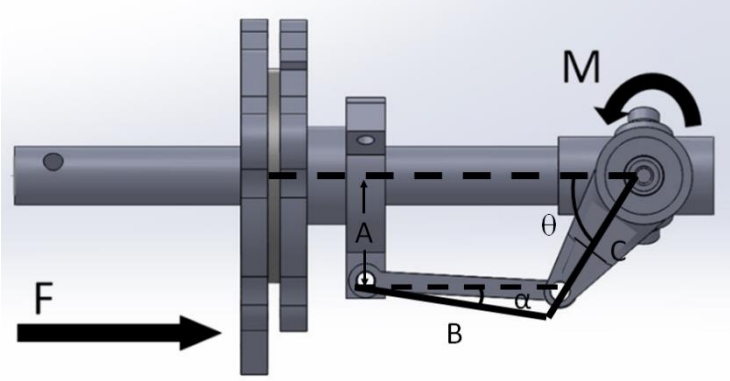

Figure 3.9 Forces applied on pitching mechanism

could be created to determine the force as a function of angle.

$$F = \frac{3Mcos(\alpha)}{Csin(\alpha + \theta)} \qquad M \approx C_m \left(\frac{1}{2}\rho U_{rel}^2\right) c^2 b$$

Equation 3.1 *Equation 3.2*

The pitch moment was determined using the assumed worst-case scenario calculated using Equation 3.2. The C_m value, coefficient of moment, used was the greatest value found over the range of attack angles through the QBlade program. Since it was only necessary to control power output up to 18 m/s, that windspeed was used. Our rated rotor speed of 2780 RPM was used for the calculation. The rotor speed and wind speed are used to calculate the relative wind speed. The density used was 0.0765 lbm/ft^3. The rest of the variables are based off the blade geometry. The chord length, c, at the root and tip were averaged to make an approximation. In Equation 3.2, b is the length of the blade from tip to root. U_{rel} was taken at the tip of the blade as a conservative approximation.

We found the necessary force to be 24.7 lbf or 109.9 N. When choosing the actuator, it was important to find one with position feedback for our control circuit. Searching through different manufacturers we found that Accutronix had the right sized actuators that still had position feedback. Based off the force found in the calculations we choose a L-12 I series actuator with the highest gear ratio rated at 100 N. Our initial calculations gave us a necessary force value of 80 N which is why an actuator with insufficient force was selected. These values would probably continue to change as more changes were made to the turbine. The stroke length needed to cover a range of angles from 40 to 130° was about 50 mm. We chose the Accutronix L-12 I because it had several different methods of control such as RC servo, voltage, and current. Figure 3.10 is a diagram of the force as it changes with pitch angle, θ.

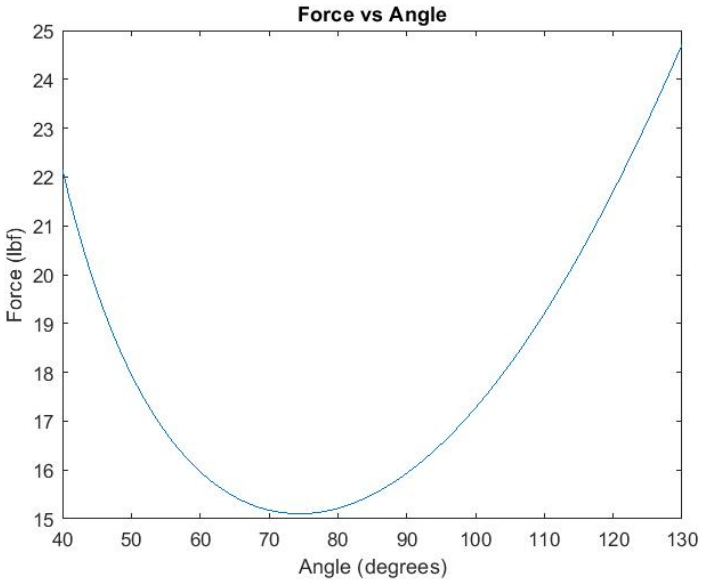

Figure 3.10 Actuator force required at each pitch Angle

Chapter 4: Generator Design

4.1 Overview

All previous Cal Maritime teams have selected commercially available motors for the power generating component of the turbine. This is common practice for many CWC teams and has helped alleviate some of the challenges that come with being a small team. However, these commercially available motors were not the ideal machine for the job for a few reasons.

Commercial motors are fairly cheap and readily available, but they are not well suited to generate power at low wind speeds. Motors are intended to be used with a constant electricity source to drive them at an optimum speed, and for this reason, they are not designed to mitigate the phenomenon of "cogging." Cogging is a resistive torque generated from the interaction

between ferrous metal and a magnetic field. Although this interaction may be neglected for a motor application or even a generator at high speed, the drawbacks of a high cogging effect are especially prominent for the startup of a small turbine. The torque necessary to spin the turbine must overcome not only the frictional resistance, but also the cogging torque.

Another major advantage of a self-fabricated design is the ability to optimize the power curve of the turbine. This is especially noticeable at low wind speeds, where the design can directly impact performance. At the 2017 CWC, Penn State demonstrated the advantage of utilizing a custom generator design with little to no cogging, winning the turbine cut-in portion of the competition, and later winning the overall competition[7]. Inspired by the advantages that a custom generator offered, the team at Cal Maritime researched different possibilities to fabricate a generator with minimal internal power loss and low inertia in the rotor.

The two conceptual designs considered were a radial and an axial flux topography. Both designs were prototyped and manufactured using 3D printing technology and tested in our wind tunnel at school. It was found that the radial flux design was generally more efficient as it allowed for more windings at a thicker wire gage, reducing copper losses. For this reason, a radial flux design was optimized for the final turbine.

In designing the final generator that was to be used in the 2020 CWC, various radial flux designs were manufactured to test manufacturing techniques and increase power generated. Traditional subtractive manufacturing techniques were explored but were not sufficient due to the rapid prototyping nature that this project took on. Instead, FDM 3D printing, an increasingly popular additive manufacturing method, was used to expedite parts manufacturing and material testing.

During testing, it was found that smaller generators typically performed better in the wind tunnel due to superior aerodynamics. To keep the turbine unit compact, the generator was limited in size, and so smaller magnets were used. To increase the magnet flux produced by these smaller magnets, a ferromagnetic core can be used as a stator to straighten out the magnetic flux or the magnets can be arranged in a Halbach array configuration. After initial experimental construction, it was decided that a Halbach array was optimal to increase the magnetic flux exposure at the face of the stator.

4.2 Radial Flux Design

A radial flux generator is designed to have permanent magnets fixed to the rotor with stationary field coils wrapped around the stator to direct the magnetic flux radially towards the coils, perpendicular to the shaft. The small and light magnets used for the rotor reduced rotational inertia and consequently decreased cut-in speed. The final design has 12 coil slots in conjunction with 10 magnetic poles. Our primary magnets are N52 2” x ½” x ¼”, which produce 3,839 Gauss (at magnet surface) each. But when the magnets were moved 0.3 inches away, the magnetic flux density dropped down to 983 Gauss. By rearranging the magnets into a Halbach array configuration, the magnetic field was strengthened while keeping the reduced size of the rotor. (See Figure 4.1) In a traditional magnetic array, the alternating magnetic polarities create equal strength magnetic fields on both top

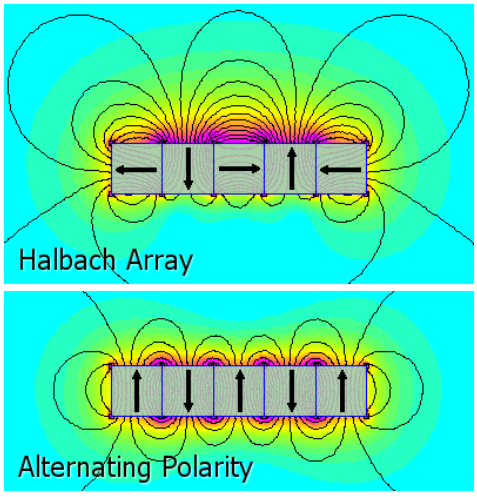

Figure 4.1 Magnet Configurations[8]

and bottom of the magnet. With the unique Halbach-array configuration that was used, smaller secondary magnets are inserted between the traditional magnetic array in a direction that is alternated by 90 degrees. The secondary magnets are N52 2” x ¼” x ⅛”, and produce 3736 Gauss (at magnet surface) each. The Halbach array transforms the magnetic field to one side of the magnet while reducing the strength on the other side to significantly increase the overall magnetic field strength exposed to the coils. As seen in Figure 4.1, comparing the alternating polarity and the Halbach array configuration, there is a significant difference between the magnetic field strength. Using the unique Halbach array magnet configuration would allow the generator to efficiently produce more power using a smaller design. (See Figure 4.2)

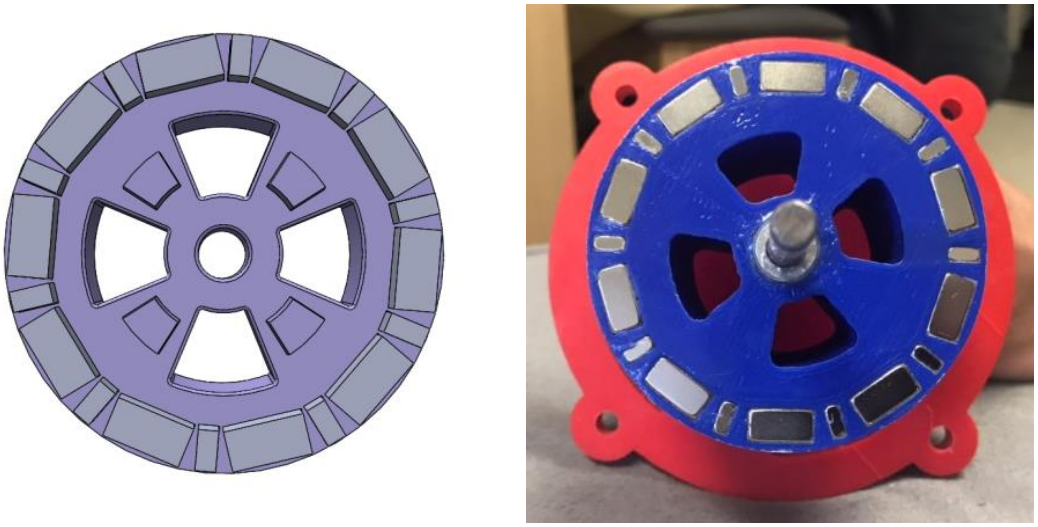

Figure 4.2 Halbach Array magnet configuration SolidWorks (left) & Actual (right)

The generator incorporated a modular design to allow for servicing of parts in case of failure or part testing. This modular design featured minimal use of adhesives by incorporating press-fitted parts. The spools, where wire coils are wound, included a dovetail type design to hold the spools firmly in place, while still allowing for easy accessibility. (See Figure 4.3)

Figure 4.3 Dovetail Spool Design

4.3 Wire Testing

Select gauges of wires were tested to determine the current threshold relative to thermal loads on the PLA components. Thin wires would increase power generated due to increased coil

turns, but they also increase resistive heating that could negatively impact the safe operation of the turbine unit. The ultimate goal of the generator was to produce a high power while keeping cut-in speed low. According to Faraday's Law, using 22 AWG was more advantageous in terms of energy generation because the generator would produce more voltage. Higher voltages at the same amount of power have less copper losses. When compared to 20 AWG, 22 AWG being thinner allows for a higher voltage but also a higher resistance and increased heat generation. Although there is less copper loss due to the low current when using 22 AWG wire, the increased heat generation adds power loss. Nonetheless, the generator needed to be able to handle increased loads and current under the CWC testing conditions of wind speeds upwards of 20 meters per second. Two wire sizes, 20 AWG and 22 AWG were tested, each having their own advantages and disadvantages that made it difficult to decide between which to use. The testing condition was simulated with no air cooling by running 2 amps for 30 minutes between two test coils, one wrapped with 20 AWG and the other with 22 AWG. Both coils were hot to touch, but the 22 AWG test coil had warped the PLA, while the 20 AWG test coil had not warped the PLA. (See Figure 4.4) Ultimately, the 20 AWG was chosen for final design to ensure that the generator would not warp during operation.

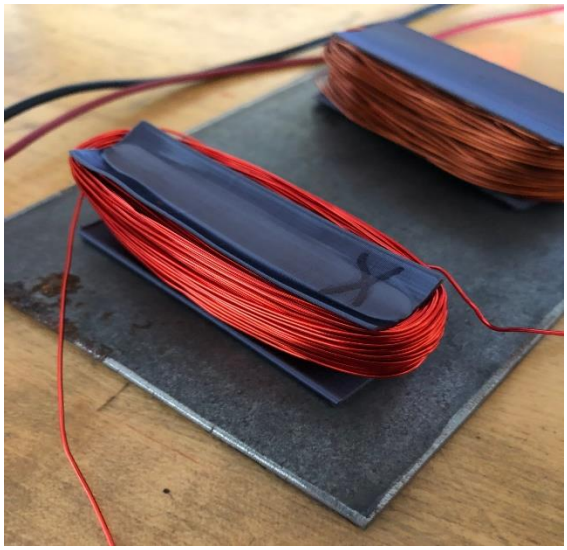

Figure 4.4 22 AWG Wire Testing

4.4 Filament Testing

Due to the high forces that this generator may be subject to during operation, the strength of the material needed to be tested in the circumstances the plastic may deform and fail. Several different filaments, including Polylactic Acid (PLA), iron-infused PLA, and Polyethylene Terephthalate Glycol-modified (PETG), were tested to ensure adequate strength during operation. It was decided that the material properties of PLA would suffice for the CWC. Although PETG provides a higher factor of safety, it was not readily available at the time of construction and requires time consuming fine tuning of the 3D printer. If a second prototype were to be produced, it would most likely have been created from a combination of PETG for its strength properties and iron infused PLA for its magnetic permeability properties.

4.5 Final Design

The generator was designed using constraints of 5 inches for the stator diameter and a maximum axial length of 5.5 inches to fit the overall turbine unit's compact design. The final radial flux generator was designed with 12 coils and 10 poles (Fig 4.7). A total of 20 magnets were used in the Halbach array to create 10 distinct poles. Figure 4.6 is a representational wiring diagram that depicts the three phases: Phase A (Red), Phase B (Blue), Phase C (Black). The air gap between the rotor and the face of the coil spools was 0.325 millimeters. Although getting the air gap to such a tight tolerance was labor-intensive, it ensures that there is no contact between the rotor and any other parts, while optimizing the magnetic flux exposed to the coils.

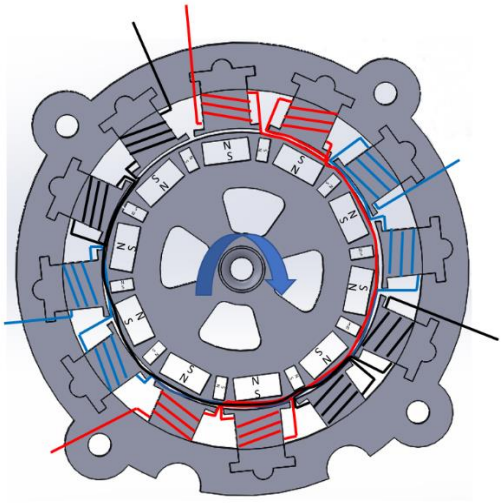

Figure 4.6 Electromagnetic Diagram – Idealized Phase Peak for Phase A

Two radial flux generator designs were produced, one with regular PLA filament and the other with a combination of iron-infused PLA filament and regular PLA filament. Between the two tests, the generator with regular PLA filament, pictured in Fig 4.7, provided the best balance between low moment of inertia and high efficiency. The generator that incorporated iron-infused PLA filament could produce more power at the same wind speed, but the cut-in wind speed was greatly increased by the exaggerated effect of cogging from the iron filament.

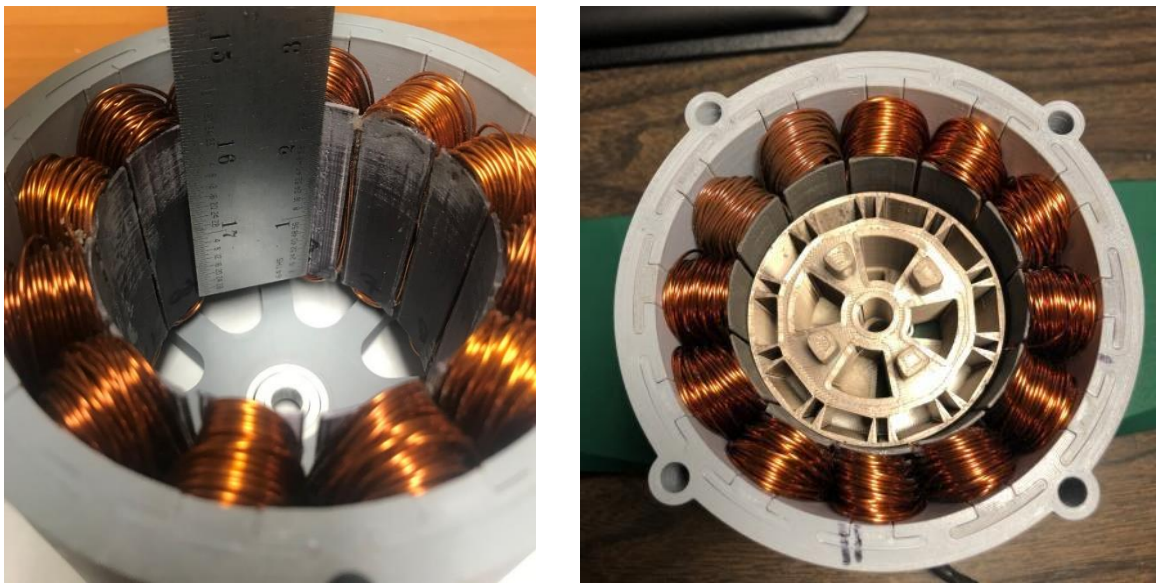

Figure 4.7 Regular PLA (left) vs Iron-Infused Spool (right)

4.6 Testing Results

Table 4.1 below displays notable test results obtained while testing the generator in the wind tunnel at Cal Maritime using the 2019 rotor.

Magnetic Gauss measured at rotor surface	3471 G
Voltage Constant (Actual)	0.020 V/RPM
Voltage Constant (Theoretical)	0.0501 V/RPM
Measured Armature Resistance	2.7 Ω
Power Gen at 8 m/s (100 Ω load)	17 W
Power Gen at 8 m/s (100 Ω load)	34 W
Copper Loss at 8 m/s	0.72 W
Cut-in Wind speed (No Load)	2.3 m/s

Table 4.1 Experimental generator test results

The results of these tests showed that the generator design was successful. The power output was about the same as the generator used in the 2019 competition, but the cut-in wind speed was reduced to 2.3 m/s from 6.2 m/s which was the primary goal behind the development of this generator[1]. One more iteration of this generator will be designed with fewer turns per coil to reduce the voltage constant and a larger shaft to match the variable pitch assembly. The most recent iteration of the design is show in Figure 4.8.

Figure 4.8 Completed Generator: SolidWorks (left) & Actual (right)

4.7 Theoretical Analysis

A theoretical analysis was completed on this generator to determine if theoretical equations could be used to accurately predict the performance of a generator before it was built. This analysis was completed using resources for axial flux generator design[9].

Equation 4.1 is used to calculate the characteristic voltage constant in DC Voltage per RPM. Where N is the number of turns per coil, B_{max} is the flux density at the face of a magnet, A is the area of the coil, p is the number of magnet poles, q is the number of coils per phase, and k_w is the winding factor.

$$\frac{V_{DC}}{n} = \frac{\sqrt{3}}{20} N B_{max} A p q k_w$$

Equation 4.1

Using Gauss measurements taken on the rotor, the winding factor of our generator topography, as well as the number of poles, coils, and turns per coil, a design voltage constant of 0.0505 V/RPM was determined. Although this voltage generated would have been excessive at operating speeds, when built the generator only recorded a voltage constant of 0.02 V/RPM when ran with no load. The major discrepancy could be linked to the way the magnetic flux

varied at the face of the coil. Because the magnets were roughly 1mm from the face of the coils, the magnetic flux would drop off considerably in a Halbach arrangement. Also, due to their rectangular nature, the flux would also vary circumferentially. Axial variations in flux were also measured, but not expected. This discrepancy in calculating a voltage constant could be mitigated by using a more accurate modelling software, such as MMS or EM works, however we were not able to complete this analysis.

Because the generated voltage would likely still be excessive at operating speed, a voltage regulator would be necessary.

Chapter 5: Electrical Design & Analysis

5.1 System Overview

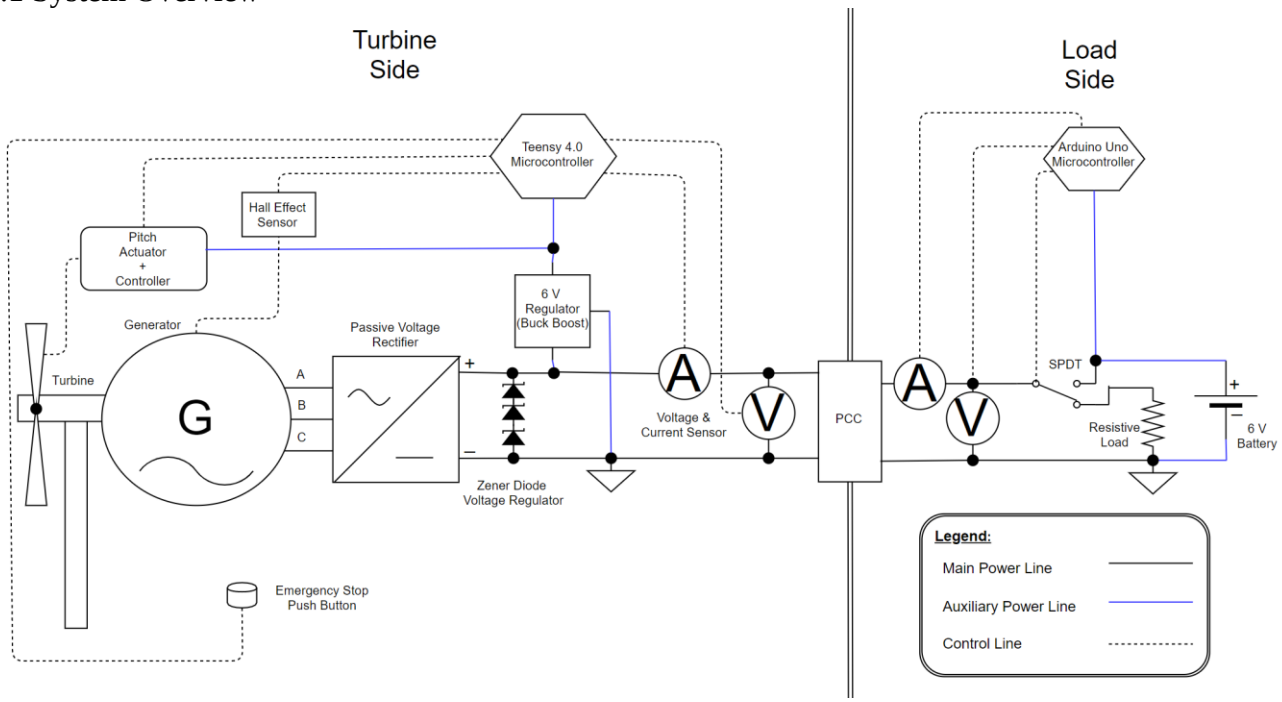

Figure 5.1 Electrical system diagram

The electrical system used in the wind turbine is shown in Figure 5.1. This system was created around the variable pitch blades. The system is divided into two sides, the turbine side and the load side. The two sides are connected by the Point of Common Coupling (PCC).

The turbine side includes the following electrical instruments: our AC generator, a passive rectifier, a 45 V Zener diode voltage regulator, a store-bought 6 V buck-boost voltage regulator, a Teensy 4.0 microcontroller, a L12 pitch actuator/controller, a Hall effect sensor, a current sensor, and a voltage sensor. Driven by the turbine's shaft, the generator produces a 3-phase, AC voltage. The voltage will be transformed into DC voltage via a passive rectifier built into a PCB. A Zener diode voltage regulator is implemented to maintain the voltage of the generator under 48 Volts. The voltage regular consists of 3 Zener diodes in series with breakdown voltages of 15 Volts each which limits the voltage received by the PCC to 45 Volts. A purchased buck-boost voltage regulator is then used to lower the voltage further into a usable 6 Volts to power the Teensy 4.0 microcontroller and pitch actuator. The microcontroller is the heart of the system, setting the pitch of the blades by controlling the pitch actuator. A closed-loop feedback system is in place to regulate the power output of the turbine system by

continually adjusting the position of the actuator so that the blades are at the desired pitch relative to the wind speed. The microcontroller monitors the power output by reading the voltage and current sensors as well as the generator's RPM.

The main power dissipating element of the load is a ceramic resistor with a fixed resistance. The load of the turbine also contains a microcontroller, a single-pole double-throw relay, a 6 Volt battery, and its own instrumentation shown in Figure 5.1. This equipment is used to restart the turbine after moving the blades to a feathered position which occurs during braking. The relay controls whether the output of the electrical system is connected to the load resistor or the battery. In the relay's off state, it is normally closed to the resistor. When needed, the load microcontroller can send a high-power signal to the relay, switching the contact over to the battery so it can be used to power the Teensy 4.0 microcontroller and the linear actuator. The instrumentation on the load side will consist of two sensors to read voltage and current. These sensors will be used by the load microcontroller to determine what state the relay should be in. The conditions that determine the state of the relay are defined in section 6.2.

5.2 Load Analysis

The optimum resistance value for the ceramic resistor was to be determined experimentally. Experience from past competitions and our own analysis tells us that the ceramic resistor will have a resistance of 48.5 Ohms and capable of dissipating at least 60W of power. A resistor was chosen for the load so only positive power could go through the PCC during the cut-in portion of the competition. When the turbine starts to cut-in, the power developed will be supplied through the PCC to the resistor before powering any peripherals allowing for points to be scored. The drawback of using a resistor is that the turbine must be able to start without active control. Also, having a fixed resistance will not allow for maximum power to be produced across all windspeeds. An appropriate resistance value needs to be selected where the power output is as a high as possible for windspeeds between 5-11 m/s.

To estimate the optimum resistance value, a MATLAB program was written to simulate the expected power to be produced at each windspeed. Turbine blade power curves were generated for each windspeed between 5-11 m/s using the nondimensionalized Cp-TSR curve for 0° pitch generated from Q-blade and the expected area swept[1]. Next, a load power curve was developed for a fixed resistance that represents the power dissipated by the resistor for a given rotor speed. To calculate the power dissipated, a DC equivalent circuit diagram was created to represent the AC generator, rectifier, and load shown in Figure 5.2. Using the experimentally determined motor constant of 20 V/1000 RPM, the current could be calculated and consequently the power. The voltage drops across the coils in the armature and across the diodes were included for a more accurate estimation of the voltage across the load. The blade power curves were overlaid on the load power curve as shown in Figure 5.3. The points of intersection represent the expected operating power and rotor speed at each windspeed. The exact resistance value was chosen by incrementally increasing the resistance and calculating how

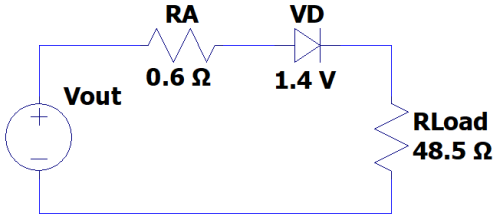

Figure 5.2 DC equivalent circuit diagram

[1] The calculations in this analysis used the properties of air at Cal Maritime. For the actual competition, the properties would be adjusted to that of the air in Denver, CO.

many points would be scored using the provided scoring guide. The resistor that scored the most points was selected. Based on the chosen constants for this analysis, a resistance of 48.5 Ω will best optimize the system. The next step is to verify the results experimentally. We expect the power output to be noticeably lower in our experimental tests as this analysis does not account for mechanical losses. The experimental results could then be used to build a more accurate analysis. It is possible a higher resistance value will need to be selected to trade points scored at the power performance task for points during the cut-in task.

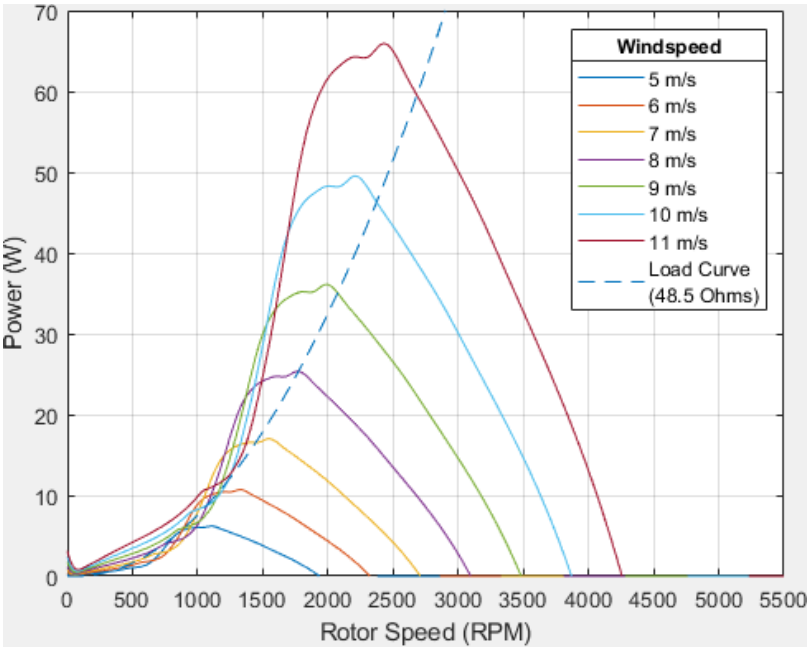

Figure 5.3 Power produced with a 48.5 Ω resistor

5.3 Actuator Pitch Range Analysis

After determining the resistance value of the load, an analysis can be performed to determine the necessary blade pitch to control the turbine at wind velocities greater than 11 m/s. From the first analysis the rated power was determined to be 57 W at a rotor speed of 2780 RPM. Changing the pitch of the blades reduces the blade efficiency and consequently the max power the blades can produce. The appropriate pitch can be determined by plotting the power curves for multiple pitch angles at a fixed wind speed using the Cp vs TSR curves in Figure 2.2 and locating where the load power curve matches one of the blade curves at 57 Watts. Figure 5.4 is an example of this process at a fixed windspeed of 14 m/s. The program iterates through multiple pitch angles until it finds a pitch angle with a power output nearest the power rated. For a windspeed of 14 m/s, the blades should be pitched at angle of -10.5 degrees for the turbine to output 57W with a corresponding rotor speed of 2600 RPM. The same analysis was performed for windspeeds between 12 and 18 m/s, and the results are shown in Table 5.1. Following the analysis, Figure 5.5 shows how the turbine is expected to perform through the power performance task and the control of rated power and rotor speed task.

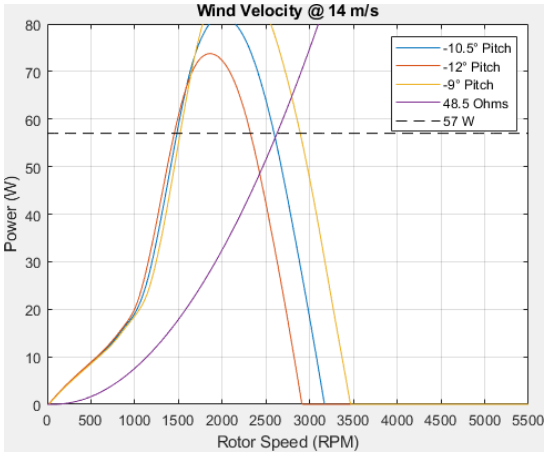

Figure 5.4 Pitch analysis example

Windspeed (m/s)	*Pitch Angle (degrees)*	*Rotor Speed (RPM)*
12	-6	2647
13	-8.5	2619
14	-10.5	2604
15	-12	2628
16	-13.5	2640
17	-15	2644
18	-16.5	2641

Table 5.1 Pitch angle to maintain rated power at each windspeed

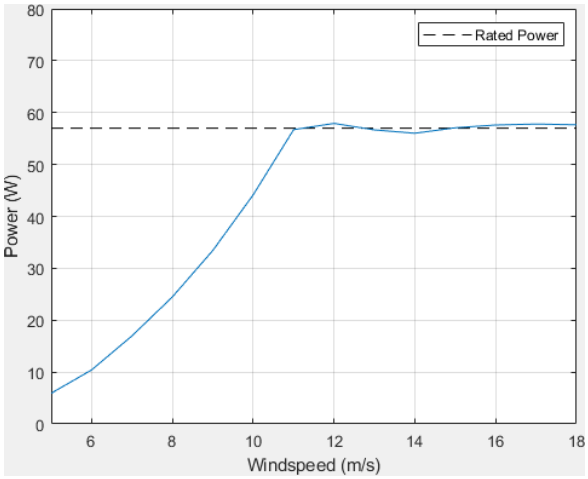

Figure 5.5 Expected power performance

Chapter 6: Controls & Analysis

6.1 System Control

The control system for our turbine starts off with passive control with the blades preset to the angle that produces the most power. The control system will maintain fixed blades until the power output monitored by the Teensy is above the rated power. The power output is calculated with data read from current and voltage sensors used in the system's instrumentation. Upon entering the power regulation state, the blades will begin to pitch to reduce the power output until it matches the rated power. As wind speed increases, the blades will pitch to maintain power at rated power while reducing rotor speed. The controls during power regulation is to be based on a proportional control scheme. Based on an experimentally determined rated power, the error between measured power out and power rated will determine how fast the actuator position changes to reach the desired power output. This control scheme is visualized in Figure 6.1. If necessary, derivative control will be added to provide damping depending on the performance of the initial control scheme. In the power regulation state, there will be a limit in the software to ensure the actuator does not pitch past zero pitch angle if windspeeds drops below 11 m/s during the durability task.

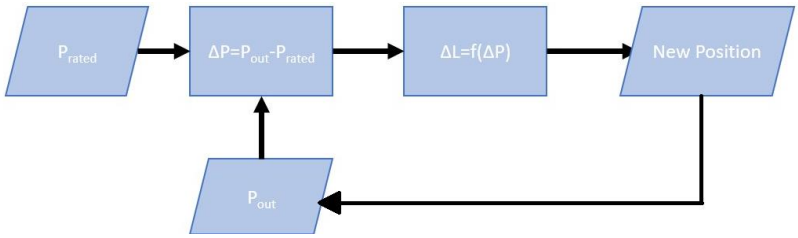

Figure 6.1 Power regulation control loop scheme

In the power regulation state, the Teensy can enter either the braking state or the cut-out state shown in Figure 6.2. The Teensy will enter the braking state when the emergency stop button is pressed or no current is detected (load disconnect) where it will feather the blades, reducing the power output close to zero. Upon the emergency stop being released or detection of current, the Teensy will enter the "start up after braking" state where it pitches the blades back to the run position. The Teensy will reenter the power regulation state when 8 volts or greater is detected. As windspeed increases, the actuator will eventually reach the cut-out position which is determined by the actuator position that is required to maintain rated power past 18 m/s. Upon reaching this position, the Teensy will enter the cut-out state and brake the turbine permanently.

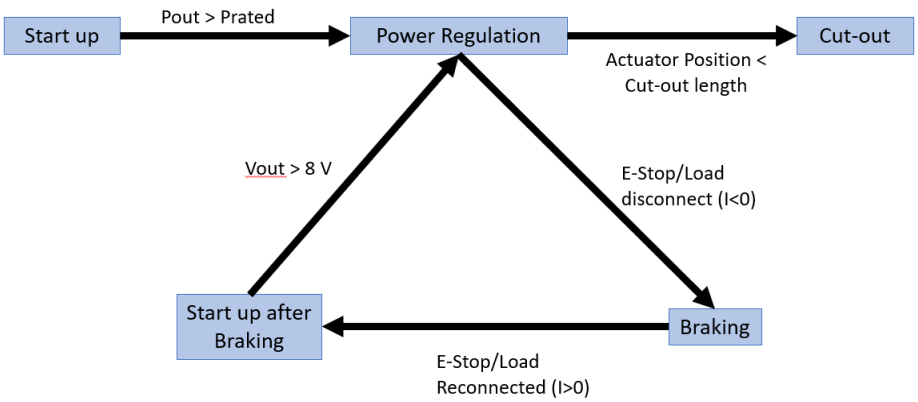

Figure 6.2 Teensy microcontroller state diagram

6.2 Safety

For a successful completion of the safety task the turbine must reduce its RPM to <10% of its rated RPM when an emergency stop is pressed or when the load is disconnected. The e-stop is a normally closed push button that will be monitored by a digital input on the Teensy. When the input reads low due to the button opening the circuit when pressed, the turbine will enter the brake state. To detect a load disconnect, the Teensy will use a current sensor. Since current cannot flow when the load is disconnected, the Teensy will read a current of 0 Amps. Upon detecting no current, the Teensy will enter the brake state commanding the actuator to feather the turbine blades.

It is also necessary the actuator to pitch the blades to a run position after a successful brake. This is accomplished with the battery in the load. During a brake condition initiated by the e-stop, the load microcontroller will detect the falling voltage with its set of instrumentation. When the voltage measured drops below 8 Volts, the load will be switched to the 6 Volt battery to allow for the actuator and Teensy to stay online. When the Teensy exits the brake state and pitches the blades for power production, the load microcontroller will switch back to the resistor after 8 Volts is being produced. During a brake condition initiated by a load disconnect, the load microcontroller will detect no current or voltage and immediately switch to the battery. When the load is reconnected, the load microcontroller will monitor the voltage as the Teensy restarts the turbine. After the voltage reaches 8 Volts the load microcontroller will switch the relay back to the resistor.

To prevent the load microcontroller from switching to the battery during the cut-in task, the microcontroller will first start in the “Do Nothing” State. In this state it will wait for the voltage it measures to surpass 10 Volts before entering the “Normally connected to load” state where it will begin to monitor for brake conditions outlined earlier. The state diagram for the load microcontroller is shown in Figure 6.3.

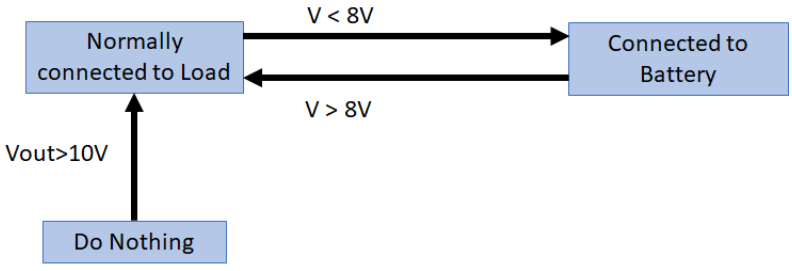

Figure 6.3 Load Microcontroller State Diagram

Bibliography

[1] Bear, N., Graham, A., Ito, D., Kizilkaya, D., Logier, R., Rodriguez, S., Sadamune, A. (2019). Technical Design Report (CWC Submission). California State University, Maritime Academy, Vallejo, CA. Retrieved from https://www.energy.gov/eere/collegiatewindcompetition/

[2] Conolly, D., Neumaier, D., Olm, A., & Williams, Q. (2018). Wind turbine design project. (Senior capstone project). California State University, Maritime Academy, Vallejo, CA. Retrieved from http://csum-dspace.calstate.edu/handle/10211.3/203207

[3] Airfoiltools.com. 2020. *RUTAN WING AIRFOIL (Amsoil2-Il)*. [online] Available at: <http://airfoiltools.com/airfoil/details?airfoil=amsoil2-il> [Accessed 26 March 2020].

[4] Manwell, J. F., McGowan, J. G., & Rogers, A. L. (2009). *Wind Energy Explained: Theory, Design and Application*. Chichester, U.K: Wiley.

[5] MITOPENCOURSWARE. 2006. *Area And Bending Inertia Of Airfoil Sections*. [online] Available at: <https://ocw.mit.edu/courses/aeronautics-and-astronautics/16-01-unified-engineering-i-ii-iii-iv-fall-2005-spring-2006/systems-labs-06/spl10b.pdf>.

[6] Young, W. C., Budynas, R. G., *Roark's Formulas for Stress and Strain*, 7th edition, 2002, McGraw Hill http://materiales.azc.uam.mx/gjl/Clases/MA10_I/Roark%27s%20formulas%20for%20stress%20and%20strain.pdf

[7] E. DeGeorge, "2017 Department of Energy Collegiate Wind Competition Technical Challenge Report," Pennsylvania State University, State College, PA, 2017.

[8] Kjmagnetics.com. 2012. *Halbach Arrays*. [online] Available at: <https://www.kjmagnetics.com/blog.asp?p=halbach-arrays> [Accessed 7 October 2019].

[9] Latoufis, K.c., et al. "Axial Flux Permanent Magnet Generator Design for Low Cost Manufacturing of Small Wind Turbines." *Wind Engineering*, vol. 36, no. 4, 2012, pp. 411–431., doi:10.1260/0309-524x.36.4.411.